PHYSICAL REVIEW C VOLUME 46, NUMBER 3 SEPTEMBER 1992

Bonn potential and *sd*-shell nuclei

M. F. Jiang
Department of Physics and Astronomy, University of Rochester, Rochester, New York 14627

R. Machleidt
Department of Physics, University of Idaho, Moscow, Idaho 83843

D. B. Stout and T. T. S. Kuo
Department of Physics, State University of New York at Stony Brook, Stony Brook, New York 11794

(Received 30 April 1991)

Using a G-matrix folded diagram method and the Bonn nucleon-nucleon potential, the s-d shell effective interaction is derived and applied to evaluate the spectra of some light sd-shell nuclei. Due to the relatively weak tensor-force characteristic for the Bonn potential, the effective interaction matrix elements, particularly those with isospin T=0, come out generally more attractive than in earlier derivations in which local, strong tensor-force potentials were used. As a consequence of this, our results for the effective interaction and the spectra are in considerably better agreement with empirical determinations and experimental data. The sensitivity of the above nuclear structure calculations to the strength of the nuclear tensor force is demonstrated systematically and the dependence of the s-d shell matrix elements on the nuclear mass number is studied.

PACS number(s): 21.30.+y, 21.60.Cs, 27.20.+n, 27.30.+t

I. INTRODUCTION

Nuclear structure predictions based on microscopic approaches, which employ the bare nucleon-nucleon (NN) potential, depend sensitively on the strength of the tensor-force component of the potential. To date, the strength of this tensor force is not well determined [1–3].

The common recipe by which NN potentials are constructed is to start from a mathematical *ansatz* that is based more or less on theory and to determine the parameters involved by a best fit to the NN scattering data below pion production threshold and the deuteron properties. It is generally agreed that for the long- and intermediate-range part of the potential, meson theory is appropriate and, in particular, all present-day potentials contain a one-pion-exchange tail. Differences between various models occur essentially at short ranges or, expressed in momentum-space language, in the off-energy-shell behavior of the potentials. Thus, the uncertainty in the strength of the tensor force concerns the short-range part of this component. The long-range tensor force is fixed by the undisputed one-pion exchange.

Most commonly employed potentials [4–6] are parametrized in terms of local functions which can be obtained in the nonrelativistic, local approximation to one-meson-exchange Feynman amplitudes. With such local expressions the empirical two-nucleon parameters sensitive to the nuclear tensor force (e.g., the deuteron quadrupole moment and asymptotic D/S state ratio, and the ϵ_1 mixing parameter up to about 300 MeV laboratory energy used in the phase-shift analysis of elastic NN scattering data) can be fit only if a relatively strong tensor force is assumed. A practical measure for the strength of the tensor-force component contained in a nuclear potential is the predicted D-state probability of the deuteron, P_D. While from nonrelativistic, local potentials [7] $P_D \approx 6\%$ is obtained (the precise values are Reid [4]; 6.5%, Paris[5]; 5.8%, Argonne V_{14} [6]; 6.1%), the Bonn potential [1,2] predicts 4.4%. The Bonn potential is based on relativistic meson theory which typically includes nonlocalities leading to a weak tensor force.

Recently, the relevance of the tensor force for the bound three-nucleon system has been investigated systematically and demonstrated clearly [1, 8]. Applying the Bonn potential, a triton binding energy of 8.35 MeV is obtained [8], while other potentials [4–6] predict about 7.5 MeV (the experimental value is 8.48 MeV). Also the other empirically known quantities of the three-nucleon system (as, e.g., the charge radius [9] and the ^{3}H-^{3}He binding energy difference [10]) fall into place for the case of the more attractive Bonn prediction.

It is a well-known fact that also the binding energy of nuclear matter is very sensitive to the strength of the tensor force [1, 11, 12]. In an energy versus density plot, the saturation points as predicted by conventional nuclear matter calculations using a variety of two-nucleon potentials are located along a band which has become known as the " Coester line" [13]. The essential parameter of this Coester band is the strength of the tensor force at low energy (as measured by P_D) with low-P_D potentials predicting more binding energy than high-P_D potentials. The typical problem with the Coester line is that when a sufficiently large binding energy is obtained, the saturation density is in general too high as compared to the empirical value. However, relativistic effects, which are repulsive and strongly density dependent, lower the sat-

uration density. Thus, applying a low-P_D potential and including relativistic effects, nuclear matter saturation can be explained rather satisfactorily [1, 14].

So far, our discussion has been concerned with nuclear ground states. Another important and interesting area are the excited states of nuclei. In a microscopic approach, one starts from a bare NN potential and derives the Brueckner G-matrix which, in turn, is used to calculate certain classes of diagrams defining the effective interaction in an open shell, V_{eff}. The matrix elements of V_{eff} can then be used to calculate, for example, the energy spectrum of an open-shell nucleus including both the ground state and the excited states.

First work along this line was done by Kuo and Brown [15], who derived matrix elements of the effective interaction between two nucleons outside an ^{16}O core. As is well known, these *s-d* shell matrix elements have been remarkably successful, at least qualitatively, in nuclear shell-model calculations. They were, however, derived some twenty-five years ago and during this time there have been developed both more realistic NN potentials and more systematic many-body methods for calculating these matrix elements. It should be worthwhile, then, to incorporate these improvements into the calculation. An attempt in this direction has been carried out by Shurpin, Kuo, and Strottman [16]. They performed a folded-diagram calculation of these matrix elements using both the Reid and Paris NN interactions. The resulting matrix elements and the energy spectra seem to have a general deficiency when compared with the recent and highly successful empirical matrix elements of Wildenthal [17]. As will be illustrated shortly, a main problem appears to be that, in general, there is not enough attraction provided by the calculated matrix elements. This fact was stressed recently also by Daehnick [18] who found, particularly, for the T=0 matrix elements a large and systematic discrepancy between theory and experiment due to a general lack of attraction on the theoretical side.

In the quoted theoretical work, conventional, local, strong-tensor-force NN potentials were used. In view of the problems mentioned, it is natural to raise the question of how sensitive the effective interaction is with regard to the bare two-nucleon potential used as input in these calculations. As discussed, in particular, there is latitude in the strength of the tensor force. Therefore it should be worthwhile to examine the influence of the strength of the bare two-nucleon tensor force on the theoretically derived effective interaction and its resultant energy spectra.

Thus, in the present work, we will use the Bonn potential to derive the *s-d* shell effective interaction [19] and then apply it in the calculation of the spectra of some light *s-d* shell nuclei. As discussed, the particular feature of the Bonn potential relevant to this application is its weak tensor force. To further investigate this aspect, other versions of this potential have been constructed [1], in which the strength of the nuclear tensor force is varied systematically. In the subsequent discussion, we will denote the original Bonn potential by Bonn A ($P_D = 4.4\%$) while the stronger tensor-force versions will be denoted by Bonn B and C ($P_D = 5.0\%$ and 5.6%, respectively). (See Ref. [1] for more details concerning the potentials.)

Another interesting aspect is the A-dependence of the effective interaction (where A denotes the nuclear mass number). In a recent study of the A=17 to A=39 nuclei, Wildenthal *et al.* [17] used the following law:

$$M(A) = M(18)(18/A)^{0.3}, \tag{1}$$

where $M(A)$ denotes a matrix element of the effective interaction for a nucleus with the mass number A. This formula implies that the strength of all matrix elements decreases with the mass number, the cause of which is assumed to be the mass dependence of the nuclear basis states [17]. Note that the very successfully empirical analysis by Wildenthal *et al.* is based on the above law. Therefore, it is of interest to examine the A dependence in a microscopic model. Recently, Hosaka, Kubo, and Toki [20] have studied the A dependence for the bare G matrix in the *sd*-shell and found an average mass dependence of $A^{-1/4}$. Our microscopic calculations include besides the bare G matrix also diagrams of second order in G and folded diagrams. We will compare our result with the assumption Eq. (1) and the findings of Ref. [20].

Since the formalism applied in this work has been published in length before, we will only briefly review it in Sec. II. The results of our calculations are presented and discussed in Sec. III. Section IV contains summary and conclusions.

II. FORMALISM

In this work, we will use the folded-diagram approach by Kuo, Lee, and Ratcliff [21, 22] in which the effective interaction is expressed as a series in the number of folds. Namely,

$$V_{\text{eff}} = F_0 + F_1 + F_2 + F_3 + \cdots , \tag{2}$$

where F_n denotes a $(n+1)$ $\hat{Q}$-box term (see below) connected with n sets of folded lines. For example, the three-times folded term has the form

$$F_3 = -\hat{Q}' \int \hat{Q} \int \hat{Q} \int \hat{Q}, \tag{3}$$

where $\int$ stands for a generalized folding operation. $\hat{Q}$ is in principle an infinite sum of irreducible diagrams while $\hat{Q}'$ is obtained from $\hat{Q}$ by removing terms of first order in the reaction matrix G. The calculation of $\hat{Q}$ can only be made approximately by selecting certain classes of diagrams. We include in the $\hat{Q}$ box all the 2-body and 1-body valence irreducible diagrams up to second order in the model-space G matrix, i.e., diagrams D1–D7 of Fig. 1 (see Ref. [16] for more details). Although there is no rigorous theoretical proof that the higher-order $\hat{Q}$-box diagrams could be dropped, it is however indicated in the calculation of Ref. [16] that their effects can be largely reduced when the corresponding folded diagrams are included as well.

To evaluate those diagrams of the $\hat{Q}$ box, we need first to calculate the model-space G matrix, which is defined by the integral equation

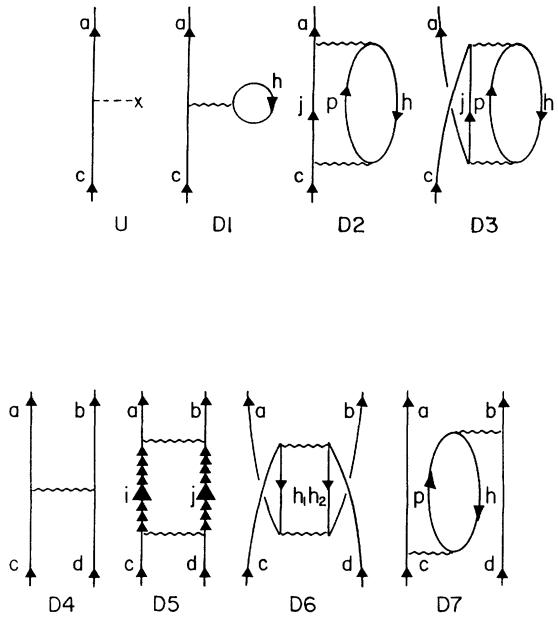

FIG. 1. $\hat{Q}$-box diagrams included in the present work. U is the single particle potential. D1–D3 are one-body diagrams while D4–D7 are two-body diagrams.

$$G(\omega) = V_{NN} + V_{NN}Q_2\frac{1}{\omega - Q_2TQ_2}Q_2G(\omega), \quad (4)$$

where Q_2 is the shell-model Pauli exclusion operator shown in Fig. 2 and T is the two-nucleon kinetic-energy operator. Using Tsai and Kuo's method [23] and a matrix inversion approach [24], the exact solution of Eq. (4) can be written as

$$G(\omega) = G_F(\omega) + \Delta G \quad (5)$$

with G_F the free reaction matrix, defined as,

$$G_F(\omega) = V_{NN} + V_{NN}\frac{1}{\omega - T}G_F(\omega) \quad (6)$$

and ΔG given by

$$\Delta G = -G_F(\omega)\frac{1}{e}P_2\frac{1}{P_2[1/e + (1/e)G_F(1/e)]P_2}P_2\frac{1}{e}G_F(\omega) \quad (7)$$

with $e = \omega - T$ and $P_2 = 1 - Q_2$.

In practical calculations, it is customary to use harmonic oscillator wave functions for the low-energy states and plane waves for the states of higher energy. The harmonic oscillator states depend on the chosen frequency parameter $\hbar\omega$. As we will discuss below, this introduces the dependence on the nuclear mass number A.

Once the effective interaction is obtained, the spectra of light *sd*-shell nuclei can be calculated by a diagonalization procedure. In our work, we employ the shell-model code developed by the Rochester–Oak-Ridge Collaboration [25].

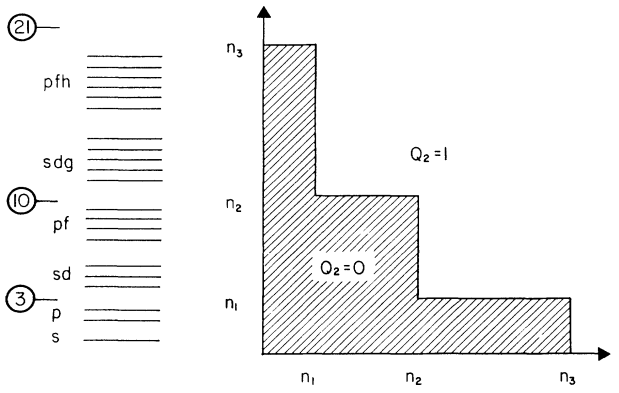

FIG. 2. Pauli exclusion operator Q_2 used in the calculation of the model-space reaction matrix G.

III. RESULTS AND DISCUSSION

A. Matrix elements

Applying the formalism outlined in the previous section and using the numerical methods described in Refs. [16, 24], we have first calculated the folded-diagram *sd*-shell effective interaction. For the bare NN interaction we employ the energy-independent one-boson-exchange parametrization of the Bonn potential of Ref. [1], which we will denote by Bonn A (P_D = 4.4%). This potential is derived from relativistic meson-exchange theory and defined in the framework of the Blanckenbecler-Sugar reduction of the Bethe-Salpeter equation using one-boson-exchange (OBE) terms. As mentioned earlier, the essential difference between this interaction and other commonly employed potentials lies in the strength of the tensor force. Due to relativistic nonlocal terms, the tensor force of the Bonn potential is weaker than in local parametrizations of the nuclear force. To elucidate systematically the effect of the tensor force strength on the effective interaction, we will also apply two variations of the Bonn potential with systematically increased tensor force strength, denoted by Bonn B and C (P_D = 5.0% and 5.6%, respectively) [1].

In Table I, we list some typical *s-d* shell matrix elements derived from these three potentials. Wildenthal's empirical matrix elements are shown for comparison. The sensitivity to the tensor force strength can be clearly seen. For instance, let us look at matrix element (TJ, *abcd*)=(01, 4444) first. It is –1.49, –1.24, and –1.09 MeV for Bonn A, B, and C, respectively. The weaker the tensor force the more attractive the matrix element. The result obtained from the weakest tensor force potential (Bonn A) is closest to the empitical value of –1.63 MeV.

This trend is known from nuclear groundstate calculations (e.g., triton, ^{16}O, nuclear matter; see Ref. [1] for an overview) and can be understood in terms of medium effects on the Brueckner G matrix. All realistic NN potentials are fit to the NN scattering data and the deuteron binding energy for which a certain intermediate-range attraction is required. A strong tensor force potential pro-

TABLE I. Shell model matrix elements $\langle abTJ|V_{\rm eff}|cdTJ\rangle$ (in units of MeV), as derived from the Bonn A, B, and C potentials [1]. The empirical data are from the analysis by Wildenthal *et al.* [17]. The orbital notation is $4 = 0d_{\frac{5}{2}}$, $5 = 1s_{\frac{1}{2}}$, and $6 = 0d_{\frac{3}{2}}$. For non-Hermitian matrix elements the average is given. $\hbar\omega = 14$ MeV.

T J	a b c d	A	B	C	Empirical
1 0	4 4 4 4	-2.77	-2.63	-2.60	-2.82
	4 4 5 5	-1.13	-1.06	-1.04	-1.32
	4 4 6 6	-3.51	-3.41	-3.35	-3.19
	5 5 5 5	-2.05	-1.90	-1.85	-2.12
	5 5 6 6	-0.83	-0.80	-0.79	-1.08
	6 6 6 6	-1.28	-1.21	-1.18	-2.18
0 1	4 4 4 4	-1.49	-1.24	-1.09	-1.63
	4 4 5 5	-1.02	-0.88	-0.79	-1.18
	4 4 6 6	+1.45	+1.29	+1.18	+0.72
	5 5 5 5	-3.53	-3.20	-2.98	-3.26
	5 5 6 6	+0.03	-0.01	-0.02	+0.03
	6 6 6 6	-0.76	-0.61	-0.52	-1.42

TABLE II. Individual two-body contributions contained in the $\hat{Q}$ box, derived from the Bonn A potential. D4–D7 refers to the diagrams in Fig. 1. The total is listed in column *sum*. For notation, parameters, and units see legend of Table I.

T J	a b c d	D4	D5	D6	D7	Sum
1 0	4 4 4 4	-1.72	-0.29	-0.41	-1.10	-3.52
	4 4 5 5	-0.81	-0.12	-0.10	-0.40	-1.43
	4 4 6 6	-3.41	-0.11	-0.26	-0.81	-4.59
	5 5 5 5	-2.45	-0.07	-0.07	-0.10	-2.69
	5 5 6 6	-0.66	-0.10	-0.08	-0.24	-1.08
	6 6 6 6	-0.33	-0.25	-0.30	-0.53	-1.41
0 1	4 4 4 4	-0.52	-0.55	-0.28	-0.34	-1.69
	4 4 5 5	-0.54	-0.31	-0.09	-0.20	-1.14
	4 4 6 6	+2.80	+0.13	-0.06	-0.76	+2.11
	5 5 5 5	-3.91	-0.44	-0.28	+0.21	-4.42
	5 5 6 6	-0.32	+0.12	-0.09	+0.25	-0.04
	6 6 6 6	-0.33	-0.26	-0.08	-0.11	-0.78

vides a large part of this attraction by means of a term of second order in the tensor potential. On the other hand, a NN potential with a weaker tensor component yielding a smaller second-order term will have a more attractive central force to provide the necessary attraction to fit the NN data. In the nuclear many-body system, terms of second and higher order are quenched by Pauli and dispersive effects [1]. The larger the tensor force, the larger the second-order term, and the larger the absolute value of the quenching of this attractive term (yielding a net repulsive medium effect).

Though in the free two-body channel, the tensor force plays an important role only for the $T = 0$ states (particularly, $^3S_1$-$^3D_1$), the effective interaction for the T=1 states is also affected by the tensor-force strength. This is mainly due to the core polarization diagram (diagram D7 of Fig. 1). To see this point more clearly, we tabulate the individual two-body diagram contributions to the $\hat{Q}$ box in Tables II and III. As seen in these tables, for T=1 the core polarization diagram (D7) is sensitive to variations of the strength of the tensor force, while for T=0 the bare G matrix (diagram D4 of Fig. 1) shows this sensitivity. Generally speaking, the effective interaction for the T=1 states has a weaker dependence on the tensor-force strength than that for the T=0 states, as shown in Tables II and III.

Comparing the predictions in Table I with the empirical matrix elements of Wildenthal, it is clearly seen that with the weakest tensor force potential (Bonn A) the best agreement is achieved. This point becomes even more clear, when comparison is made with predictions from local strong-tensor force potentials, like Reid and Paris (Table IV). As example, let us consider the matrix element (TJ, $abcd$)=(10, 4444). The results based on the Reid and Paris potentials, -2.07 and -2.22 MeV, respectively, are significantly weaker than the Wildenthal result of -2.82 MeV, with which the Bonn A prediction of

TABLE III. Same as Table II, but for Bonn C.

T J	a b c d	D4	D5	D6	D7	Sum
1 0	4 4 4 4	-1.77	-0.30	-0.41	-0.94	-3.42
	4 4 5 5	-0.82	-0.13	-0.10	-0.35	-1.40
	4 4 6 6	-3.39	-0.12	-0.27	-0.73	-4.51
	5 5 5 5	-2.45	-0.07	-0.07	+0.03	-2.56
	5 5 6 6	-0.67	-0.10	-0.08	-0.21	-1.06
	6 6 6 6	-0.38	-0.25	-0.31	-0.39	-1.33
0 1	4 4 4 4	-0.20	-0.51	-0.21	-0.38	-1.30
	4 4 5 5	-0.43	-0.28	-0.05	-0.23	-0.99
	4 4 6 6	+2.53	+0.09	-0.09	-0.68	+1.85
	5 5 5 5	-3.49	-0.43	-0.25	+0.15	-4.02
	5 5 6 6	-0.45	+0.11	-0.09	+0.28	-0.15
	6 6 6 6	+0.00	-0.24	-0.08	-0.10	-0.42

TABLE IV. Shell model matrix elements $\langle abTJ|V_{\rm eff}|cdTJ\rangle$ (in units of MeV) calculated from the Bonn A [1], the Paris [5], and the Reid potential [4]. Notation as in Table I.

T J	a b c d	Bonn A	Paris	Reid	Empirical
1 0	4 4 4 4	-2.77	-2.22	-2.07	-2.82
	4 4 5 5	-1.13	-0.89	-0.88	-1.32
	4 4 6 6	-3.51	-3.09	-3.05	-3.19
	5 5 5 5	-2.05	-1.61	-1.47	-2.12
	5 5 6 6	-0.83	-0.69	-0.69	-1.08
	6 6 6 6	-1.28	-0.95	-0.85	-2.18
0 1	4 4 4 4	-1.49	-1.01	-1.01	-1.63
	4 4 5 5	-1.02	-0.67	-0.56	-1.18
	4 4 6 6	+1.45	+1.12	+0.92	+0.72
	5 5 5 5	-3.53	-2.73	-2.63	-3.26
	5 5 6 6	+0.03	-0.06	-0.07	+0.03
	6 6 6 6	-0.76	-0.51	-0.53	-1.42

-2.77 MeV is in close agreement. For the $(TJ, abcd)$=(01, 4444) matrix element the situation is quite similar. The better agreement is in general due to an increase of attraction.

In this work, the convergence properties of the folded diagram series have also been studied. Terms up to $\tilde{F}_4$ are displayed in Table V (for the exact definition of $\tilde{F}_n$ see Ref. [16]). It is seen that the contributions from the three plus four folds are very small. Thus, in agreement with earlier findings [16], the folded-diagram series appears to converge rather satisfactorily. A previous study using the Bonn potential [26] has also shown that a weaker tensor force potential has a negligible Vary-Sauer-Wong effect [27], leading to better convergence.

The overall improvement on the theoretically derived effective interaction can be seen in the total χ^2 [28] calculated for the 63 matrix elements (see Table VIII of the Appendix) which is 20.1, 24.9, and 25.3 MeV^2 for Bonn A, Reid, and Paris potentials, respectively. For the T=0 matrix elements only, it is 15.0, 17.5, and 18.5 MeV^2, and for $T = 1$ one obtains 5.1, 7.4, and 6.8 MeV^2, again, for Bonn A, Reid, and Paris potentials, respectively.

We should note that some of the calculated matrix elements still lack attraction. An example is the [6666] multiplet. Though the Bonn A prediction is more attractive than any other, still substantial attraction is missing in this case (cf. Tables I and IV). It appears that large differences occur mostly for the matrix elements which involve the $d_{3/2}$ orbit. A possible reason for this is the following. First, this orbit is nearly unbound and it is probably not well represented by a harmonic oscillator wave function. More realistic would be a wave function derived from a Woods-Saxon potential or obtained in a Hartree-Fock calculation.

A more pertinent reason may be the following. The s.p. (single-particle) energies are treated as adjustable parameters in Wildenthal's calculation, while in our folded-diagram formalism we are supposed to use the A=17 experimental s.p. energies whose relative spectrum is (0, 0.87, 5.08) MeV for the orbit 4, 5, 6, respectively. In contrast, the corresponding "best-fit" s.p. energies used by Wildenthal are (0, 0.78, 5.59) MeV. In fact, the total two-body effective Hamiltonian H_{eff}, i.e., the sum of the s.p. energies and the effective interaction matrix elements, for the [6666] multiplet given by our calculation is actually quite close to that of Wildenthal. The above comparison may have brought with it an important message concerning the many-body forces which have not been taken into account in our derivation. The above multiplet involves only two valence nucleons and we have reproduced Wildenthal's H_{eff} well. Many-body effective forces are not involved in this case. However, when there are more than, e.g., two $d_{3/2}$ nucleons, such forces may be needed in order to reproduce Wildenthal's H_{eff}. We feel that Wildenthal's choice of the s.p. energies contains, to some extent, an effective way to compensate for the many-body forces which have not been considered in his empirical matrix elements.

TABLE V. Representative V_{eff} matrix elements in the $\tilde{F}_n$ series (using the Bonn A potential). Notation, parameters, and units as in Table I; $\tilde{F}_n$ as defined in Ref. [16].

T J	a b c d	$\tilde{F}_0$	$\tilde{F}_1+\tilde{F}_2$	$\tilde{F}_3+\tilde{F}_4$	V_{eff}
1 0	4 4 4 4	-3.52	+0.60	+0.15	-2.77
	4 4 5 5	-1.43	+0.23	+0.06	-1.14
	4 4 6 6	-4.59	+0.94	-0.00	-3.65
	5 5 5 5	-2.69	+0.56	+0.08	-2.05
	5 5 6 6	-1.08	+0.26	+0.02	-0.80
	6 6 6 6	-1.41	+0.07	+0.06	-1.28
0 1	4 4 4 4	-1.69	+0.13	+0.07	-1.49
	4 4 5 5	-1.14	+0.12	+0.02	-1.00
	4 4 6 6	+2.11	-0.83	+0.07	+1.35
	5 5 5 5	-4.42	+0.79	+0.10	-3.53
	5 5 6 6	-0.04	+0.01	-0.01	-0.04
	6 6 6 6	-0.78	-0.03	+0.05	-0.76

B. Spectra

Besides the comparison with so-called empirical matrix elements, it may be instructive to also compare directly with the experimental data. For that purpose, we have calculated the spectra of some light *sd*-shell nuclei (Fig. 3). These spectra are calculated using the above-derived *sd*-shell effective interaction with an A dependence as proposed by Wildenthal and co-workers [17], Eq. (1). In these figures, the potential predictions are arranged such that the tensor force strength (and the P_D) decreases when going from left to right (cf. Table VI). Besides the experimental spectra, we also show those obtained when using Wildenthal's empirical matrix elements.

It is evident that a number of low-lying experimental levels are not reproduced by our calculation. This is mainly because of the model space which we have chosen for our calculation. Our model space consists of a closed ^{16}O core with active valence nucleons confined in the *sd*-shell. Thus, for instance, our calculated levels for ^{18}O and ^{18}F are those whose wave functions are predominantly of 2p0h (two-particle–no-hole) nature. The states whose wave functions are mainly of 4p2h structure are not supposed to be adequately described by our model-space calculation. The experimental 3.63 MeV 0^+, 5.26 MeV 2^+, and 7.12 MeV 4^+ states of ^{18}O, see "Exp." column of the ^{18}O spectrum (Fig. 3), are well known to be

TABLE VI. Deuteron D-state probability, P_D, for the NN potentials applied in the calculation of the spectra displayed in Fig. 3.

Potential	P_D (%)
Reid [4]	6.47
Paris [5]	5.77
HM1 [29]	5.75
Bonn C [1]	5.61
Bonn B [1]	4.99
Bonn A [1]	4.38

members of a 4p2h band. Hence it is not unexpected that these states are not reproduced well by our calculation, nor by Wildenthal's calculation which is also based on a closed ^{16}O core model space. We note that Wildenthal included only the lowest 0^+, 1.98 MeV 2^+, and 3.55 MeV 4^+ states in his fit [17]. This is clearly a resonable thing to do as these states are well known to be of 2p0h nature. The second 4^+ state given by Wildenthal and by our Bonn A calculation are both at about 9 MeV, which is in good agreement with the recent measurement by Fortune *et al.* [31]; they identified that the predominantly $d_{5/2}d_{3/2}$ 4^+ level is at 9 MeV.

We now turn to the energy levels of ^{18}F (Fig. 3), which have been rather extensively studied [32]. Wildenthal included the lowest six states ("Wild." column) in his fit, as these states are generally believed to be predominately of 2p0h nature. Our calculation has given these six levels but with a much broader spread. This may indicate that the 4p2h admixture is more important in ^{18}F than in ^{18}O.

Our calculated lowest 3^+ level for ^{19}F (see Fig. 3) is too close to the ground state, as compared with Wilden-

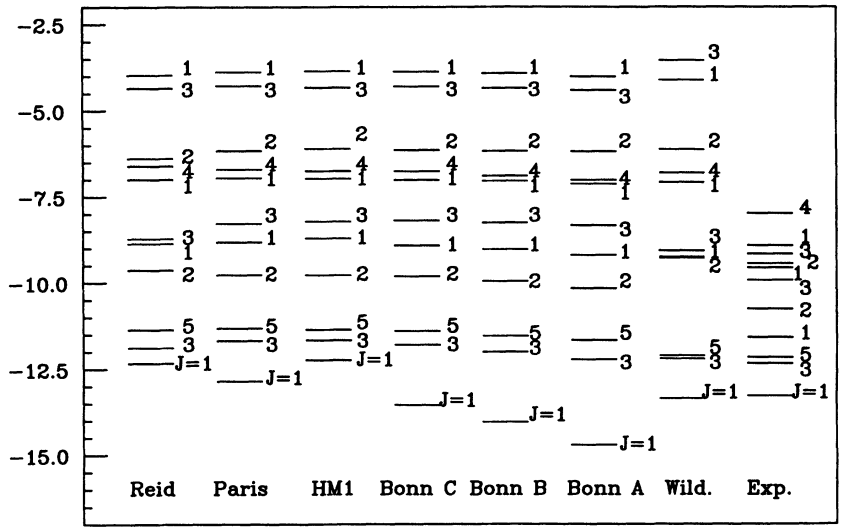

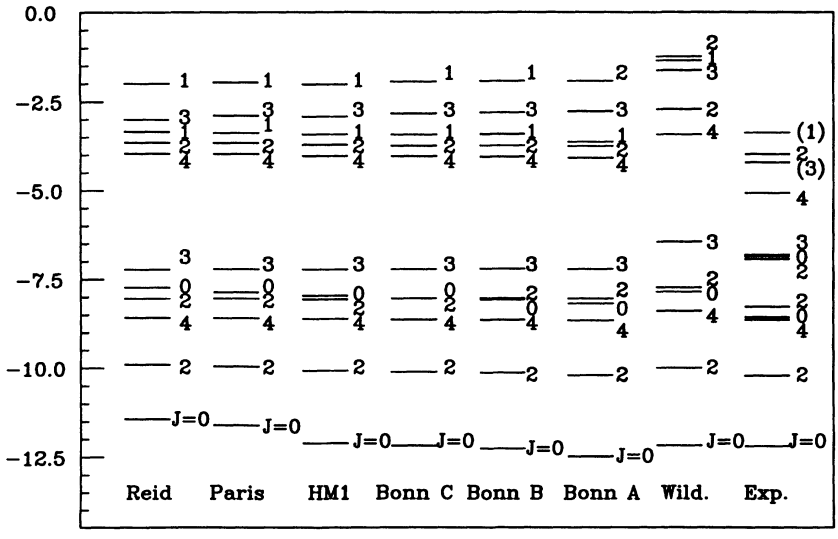

FIG. 3. Positive-parity energy spectra of some $A = 18 - 21$ nuclei. For the calculated spectra the Reid [4], Paris [5], HM1 [29], and Bonn A, B, C [1] potentials are used. The spectra obtained by using Wildenthal's empirical interaction (Wild.) [17] and the experimental data (Exp.) [30] are also shown.

thal's calculation and with experiment. Note that the second 3^+ state in the "Exp." column of Fig. 3 appears to be entirely missed by our calculation. A possible explanation is that this state is mainly an "intruder" state in the sense that its wave function is predominantly outside of the model space we have employed. The lowest 3^+ state may also have a significant amount of intruder components, and our calculation may be improved if an extended model space is used where some of the main components of the intruder state are explicitly included in the basis vectors. The low-lying states of the A=20 nuclei are rather satisfactorily reproduced by our calculations. Our results for A=21 are also reasonable.

From the above figures, a general trend is observed, namely the spectra become more attractive when the tensor force strength of the NN potential decreases. This trend can be seen in all nuclei calculated. In general there is good agreement between the spectra calculated from the Bonn A or B potential and experiment. Notice that the tensor force of the Bonn B potential (though stronger than Bonn A) is still rather weak as compared to potentials like Reid or Paris (cf. Table VI). In particular, the spectra of the heavier nuclei ^{20}Ne and ^{21}Ne are in remarkably good agreement with experiment when Bonn A is used. We also like to point to the fact that the good agreement is not destroyed when going to higher isospin levels, like ^{20}F($T=1$), ^{20}O($T=2$), or ^{21}F($T=3/2$).

Our results are consistent with those of a recent inves-

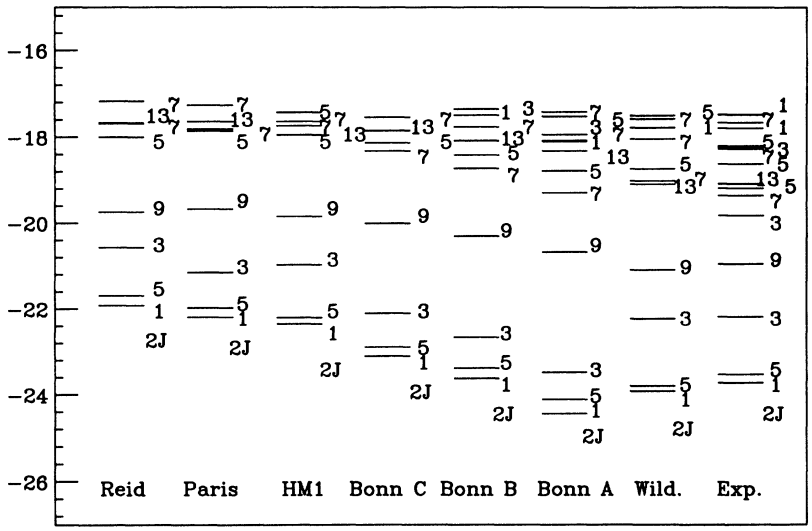

Energy Levels of ^{19}F (T=1/2) [MEV]

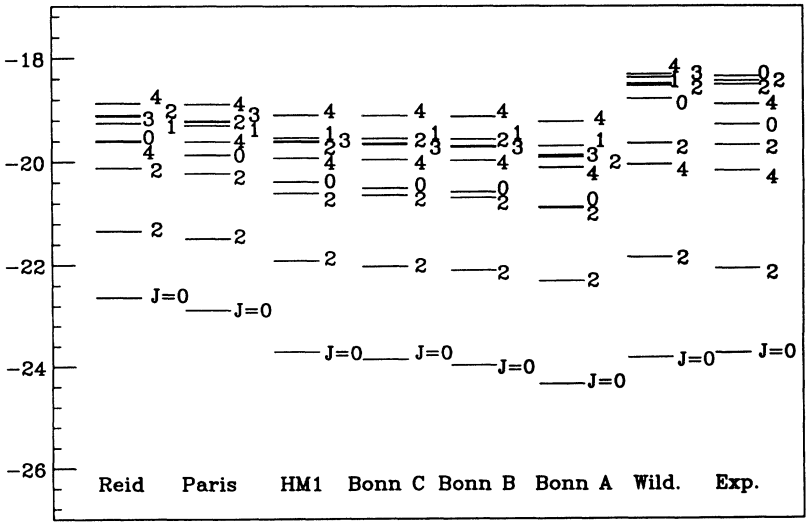

Energy Levels of ^{20}O (T=2) [MEV]

FIG. 3. (*Continued*).

tigation by Maglione and Ferreira [33], where two versions of the Bonn potential were used. The difference between Ref. [33] and the present work is that in the former study local configuration space versions of the Bonn potential are employed (while we use the original, nonlocal momentum-space versions). By comparison, we find that the spectra derived in this work are even more attractive than the corresponding ones of Ref. [33]. This indicates that nonlocality brings about extra attraction in nuclear structure calculations.

As mentioned earlier, the T=1 effective interaction has a weaker dependence on the tensor force strength than the T=0 interaction. This can be clearly seen, for example, by comparing the calculated spectrum of $^{18}O(T = 1)$ with that of $^{18}F(T = 0)$ (Fig. 3). The spectrum of ^{18}O shows a much weaker dependence on the potentials than that of ^{18}F. This is also seen in the predictions for the ground state energy. The difference between the ground-state energies obtained from the Reid and Bonn A potential is 2.5 MeV for ^{18}F while it is only 1 MeV for ^{18}O. This energy difference increases with the nuclear mass number A, and it is $\approx$4.5 MeV for ^{21}Ne. This is simply due to the fact that in a heavier nucleus there are more interacting pairs.

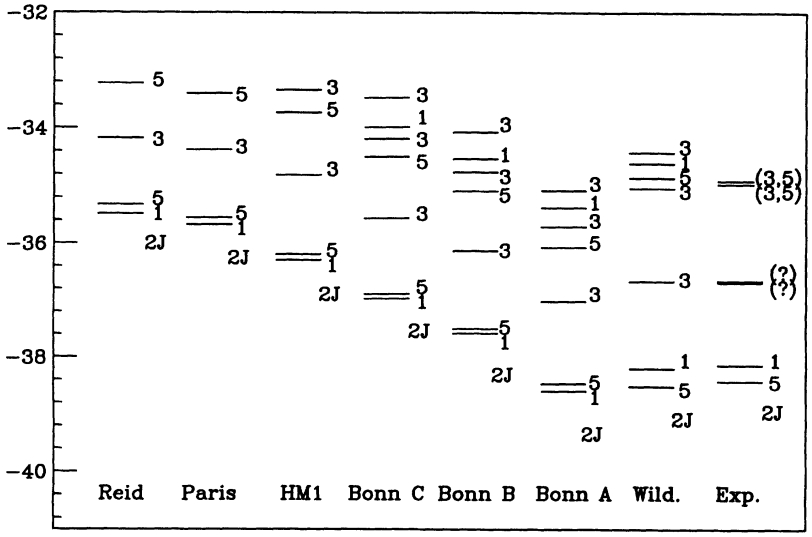

Energy Levels of ^{21}F (T=3/2) [MEV]

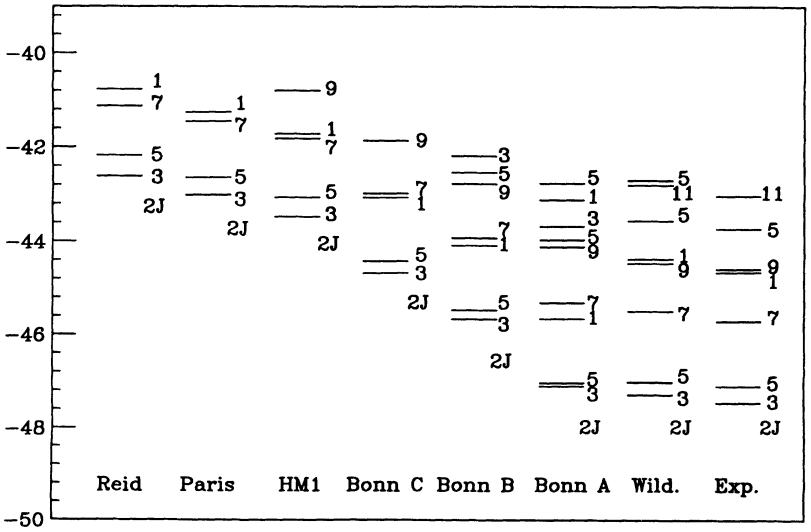

Energy Levels of ^{21}Ne (T=1/2) [MEV]

FIG. 3. (*Continued*).

C. A dependence

We turn now to the A dependence of the effective interaction. As mentioned earlier, in the present work a harmonic-oscillator single-particle (s.p.) potential is used to describe the unperturbed s.p. orbits. This s.p. potential has one parameter, namely $\hbar\omega$. The s.p. wave functions and the corresponding s.p. energies depend on this oscillator parameter. It is reasonable to assume that the oscillator parameter depends on the mass number A of the nucleus, with a larger A implying a smaller $\hbar\omega$ (corresponding to a larger nuclear radius). We use the relationship

$$\hbar\omega = 41.47A^{-\frac{1}{3}} \text{ MeV}. \tag{8}$$

Some matrix elements as a function of A are listed in Table VII. As samples, we have calculated the cases A=18, 23, 28, 33, and 38 corresponding to $\hbar\omega$=15.8, 14.6, 13.7, 12.9, and 12.3, respectively. In Fig. 4 these matrix elements are plotted versus $\hbar\omega$. It is seen that the dependence on $\hbar\omega$ (or equivalently on $A^{-\frac{1}{3}}$) is almost linear, which is in qualitative agreement with the assumption made in the empirical analysis by Wildenthal, Eq. (1).

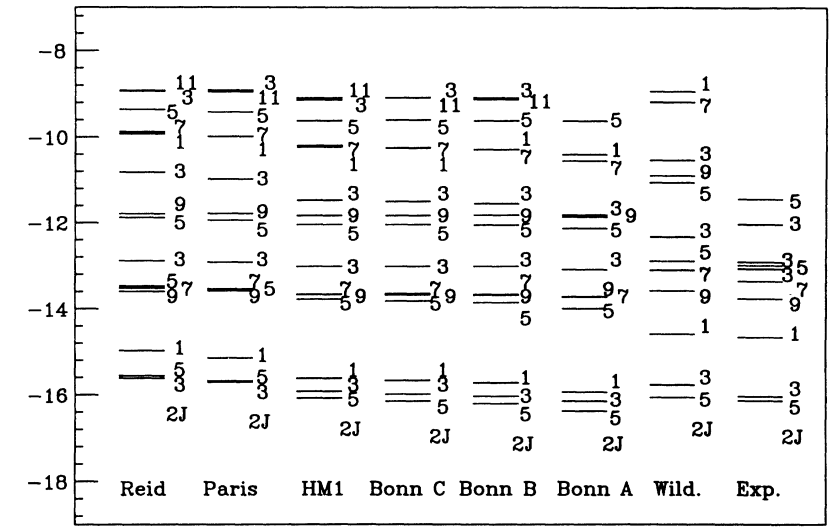

Energy Levels of ^{19}O (T=3/2) [MEV]

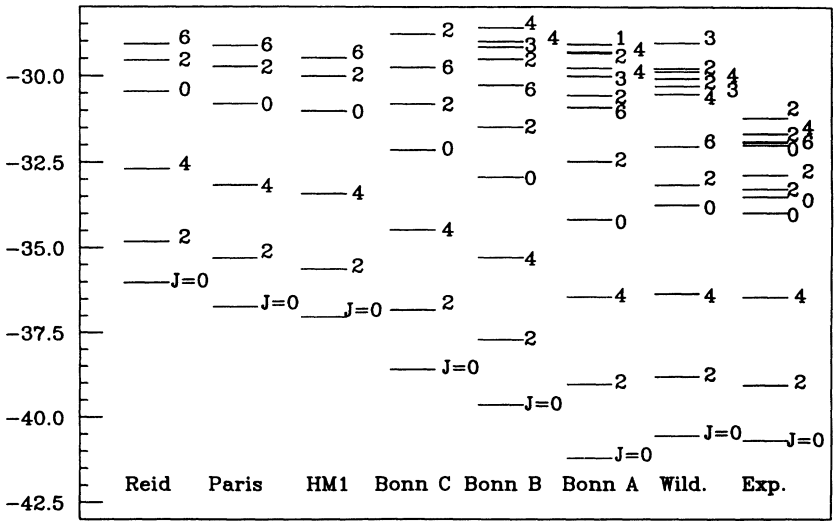

Energy Levels of ^{20}Ne (T=0) [MEV]

FIG. 3. (*Continued*).

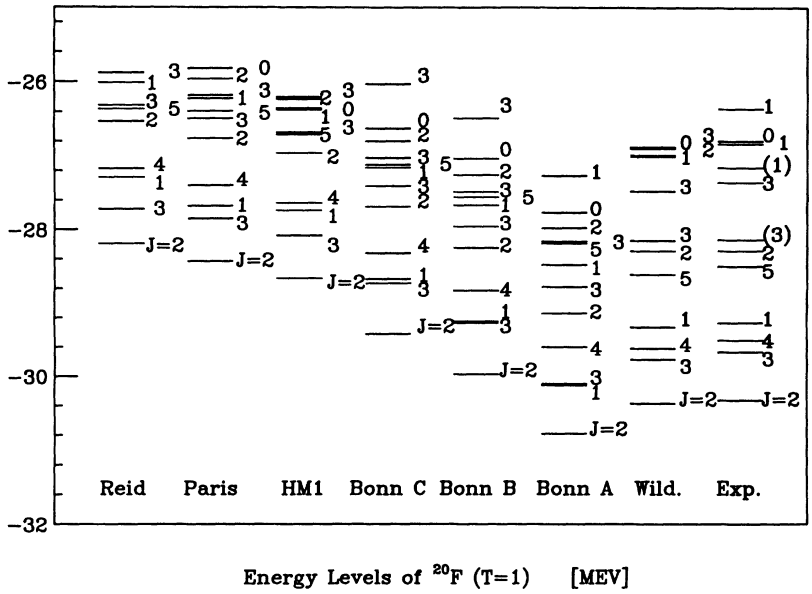

FIG. 3. (*Continued*).

This suggests that the A dependence of the effective interaction largely comes from the A dependence of the nuclear wave function or, equivalently, the s.p. mean field.

Our mass dependence of $A^{-1/3}$ is close to the $A^{-1/4}$ dependence obtained for the bare G matrix in Ref. [20]. The slight difference can be understood by considering the range of the various contributions to the effective interaction. As is known (see Brown *et al.* [17]), using harmonic-oscillator radial wave functions with $\hbar\omega$ assumed to be proportional to $A^{-1/3}$, the effective interaction for a delta interaction varies as $A^{-1/2}$ while for a Coulomb interaction it varies as $A^{-1/6}$. Thus, assuming the general form $A^{-\alpha}$, α is larger for the shorter range. Thus, the shorter range of the higher-order G matrix and folded diagrams included in our work explains the shift from $A^{-1/4}$ for the G matrix ([20]) to $A^{-1/3}$ in our calculations.

TABLE VII. A dependence of some typical matrix elements of the *s-d* shell effective interaction (derived from the Bonn A potential). For notation and units see Table I.

T J	a b c d	A=18	A=23	A=28	A=33	A=38
1 0	4 4 4 4	-2.62	-2.73	-2.79	-2.82	-2.83
	4 4 5 5	-1.10	-1.13	-1.14	-1.15	-1.15
	4 4 6 6	-3.89	-3.74	-3.61	-3.48	-3.38
	5 5 5 5	-1.99	-2.03	-2.06	-2.07	-2.06
	5 5 6 6	-0.76	-0.79	-0.81	-0.82	-0.83
	6 6 6 6	-1.11	-1.23	-1.30	-1.36	-1.40
0 1	4 4 4 4	-1.27	-1.42	-1.52	-1.61	-1.67
	4 4 5 5	-0.89	-0.96	-1.02	-1.08	-1.12
	4 4 6 6	+1.33	+1.35	+1.36	+1.36	+1.35
	5 5 5 5	-3.54	-3.54	-3.53	-3.52	-3.51
	5 5 6 6	-0.12	-0.07	-0.02	+0.02	+0.06
	6 6 6 6	-0.72	-0.75	-0.77	-0.78	-0.79

We note that there are some exceptions from the rule Eq. (1). As seen from Table VII and Fig. 4, with the increase of A (or decrease of $\hbar\omega$), the magnitude of the matrix elements does not decrease in all cases. For example, the strength of the matrix elements (TJ, $abcd$)=(10, 4444), (10, 5555), (10,6666), (01, 4444), and (01, 4455) is increasing with A, though most of them still have the linear dependence on $A^{-1/3}$. This peculiar behavior is also observed by Hosaka *et al.* [20] in studying the mass dependence of the bare G matrix. It is certainly not a surprise since the scaling law used by Wildenthal represents only an overall average for the reduction in the matrix elements as the size of the nucleus increases. But, from our microscopic calculation, it appears that a different scheme may be needed to summarize the A dependence of the *s-d* shell effective interaction. The empirical A-dependence formula of Wildenthal, as displayed in Eq. (1), seems to oversimplify the detailed A dependence of our calculated matrix elements. It should be of interest to study the effect of this calculated mass dependence on the nuclear spectra and on the fitted two-body effective interaction. It may be noted that our calculated T=1 matrix elements show a generally weaker A dependence than the T=0 ones, as can be seen from Fig. 4. This may be an indication that the nucleon-nucleon tensor force plays a role for the A dependence.

IV. SUMMARY AND CONCLUSIONS

We have derived the matrix elements for the *s-d* shell effective interaction from the Bonn potential using a *G*-

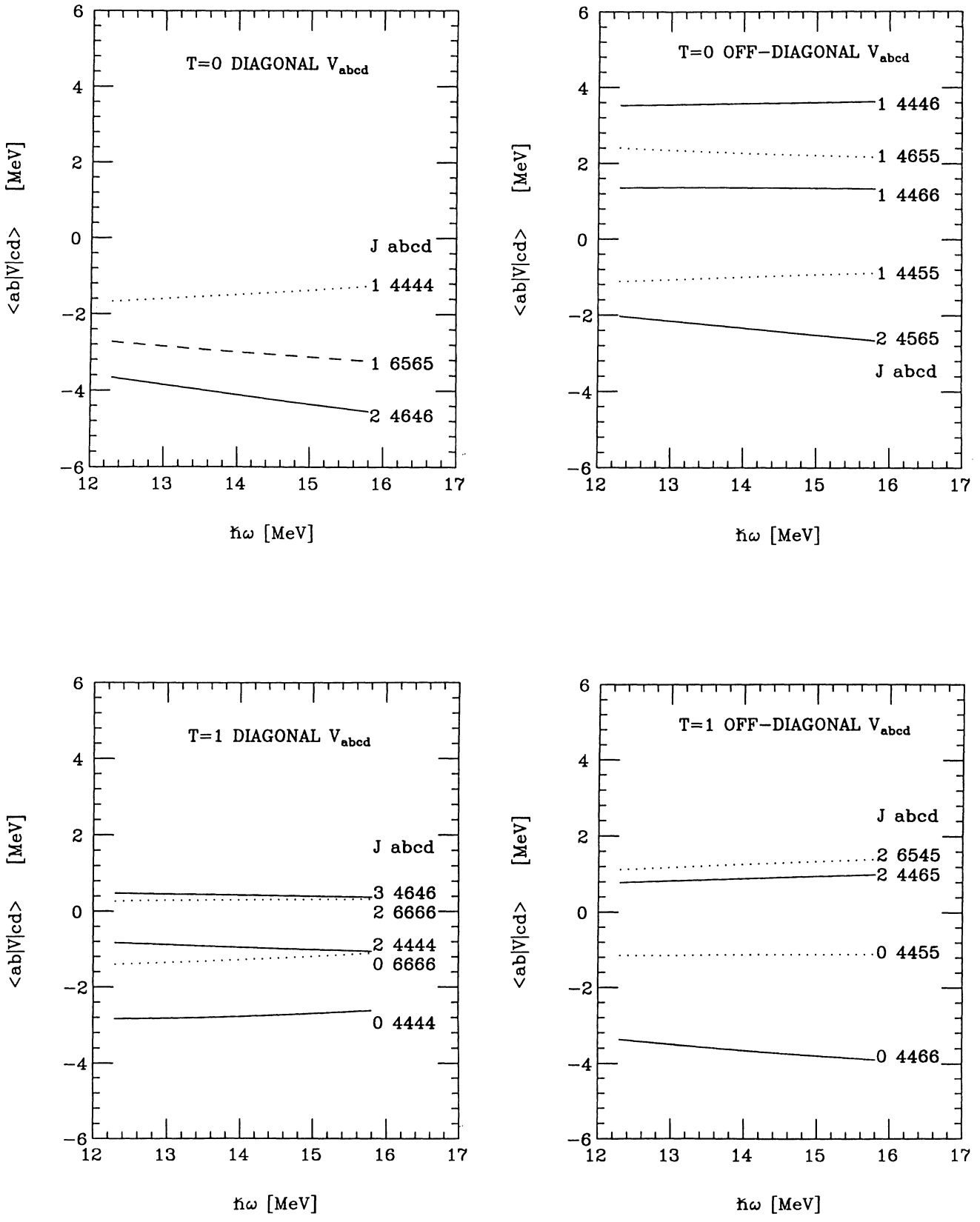

FIG. 4. *A* dependence of some typical matrix elements (using the Bonn A potential). For orbital notation see legend of Table I.

TABLE VIII. *s-d* shell matrix elements calculated from the Bonn A potential. Notation, parameters, and units as in Table I.

$TJabcd$	V_{abcd}	$TJabcd$	V_{abcd}	$TJabcd$	V_{abcd}	$TJabcd$	V_{abcd}
014444	-1.4899	024565	-2.3296	054444	-3.3831	124565	1.2664
014446	3.5445	024645	-1.3985	104444	-2.7702	124566	-0.6302
014455	-1.0178	024646	-4.1049	104455	-1.1265	124645	-0.2372
014465	0.2951	024665	-1.4808	104466	-3.5088	124646	-0.2028
014466	1.4522	026565	-1.2532	105555	-2.0511	124665	0.6953
014646	-6.4045	034444	-0.7392	106655	-0.8341	124666	-0.9748
014655	2.2509	034445	-1.5783	106666	-1.2810	126565	-0.1412
014665	1.9065	034446	1.9458	114646	-0.2191	126665	0.2636
014666	-0.2461	034466	0.6098	114665	-0.0590	126666	0.2949
015555	-3.5329	034545	-3.4145	116565	0.4112	134545	0.2104
016555	-0.5565	034566	0.0671	124444	-0.9482	134645	-0.0790
016565	-2.9886	034645	1.1185	124445	-0.8269	134646	0.4279
016655	0.0273	034646	-0.8800	124446	-0.2285	144444	0.0533
016665	-0.8229	034666	2.0155	124465	0.8472	144446	-1.3148
016666	-0.7629	036666	-2.0657	124466	-0.8947	144646	-1.2952
024545	-0.4683	044646	-3.8224	124545	-1.1223		

matrix folded-diagram method. Furthermore, we have applied these matrix elements to calculate the energy spectra of light *sd*-shell nuclei. The main result is that these matrix elements are generally more attractive than in former derivations. This increase of attraction leads to a substantially better agreement with the empirical matrix elements as well as with the experimental energy spectra. The reason for these improvements can be clearly traced to the weaker tensor force characteristic for the Bonn potential.

The present results derived from the Bonn potential together with earlier findings like, e.g., the successful prediction of the triton binding energy [1, 8] and the quantitative explanation of nuclear-matter saturation [14], may indicate that modern genuine meson-theoretic potentials allow for a more consistent and successful description of nuclear structure phenomena than traditional, simplistic (local) nuclear force models.

As a by-product of our calculations, we have also investigated the dependence of the effective interaction on the nuclear mass number A. An overall mass dependence of $A^{-1/3}$ is obtained in close agreement with the assumptions by Wildenthal *et al.*, the source of which is found to be the nuclear wave function, or equivalently, the s.p. field. There are a number of cases where the A dependence of our calculated matrix elements appears to be different from the empirical A dependence of Wildenthal. This point deserves further study in the future.

This work has been supported in part by the U.S. National Science Foundation (through the NSF-Idaho EPSCoR program under Grant No. RII-8902065, the NSF San Diego Supercomputer Center, and under Grant No. PHY-8911040) and by the U.S. Department of

TABLE IX. *s-d* shell matrix elements calculated from the Bonn B potential. Notation, parameters, and units as in Table I.

$TJabcd$	V_{abcd}	$TJabcd$	V_{abcd}	$TJabcd$	V_{abcd}	$TJabcd$	V_{abcd}
014444	-1.2359	024565	-2.2593	054444	-3.2498	124565	1.2312
014446	3.3070	024645	-1.3311	104444	-2.6360	124566	-0.6008
014455	-0.8770	024646	-4.0229	104455	-1.0640	124645	-0.2202
014465	0.2793	024665	-1.3998	104466	-3.4128	124646	-0.1957
014466	1.2933	026565	-1.1728	105555	-1.8997	124665	0.6877
014646	-6.0576	034444	-0.6294	106655	-0.8008	124666	-0.9436
014655	2.0497	034445	-1.5161	106666	-1.2074	126565	-0.1204
014665	1.9576	034446	1.8798	114646	-0.2037	126665	0.2586
014666	-0.1343	034466	0.5631	114665	-0.0399	126666	0.2834
015555	-3.1975	034545	-3.2427	116565	0.4156	134545	0.2176
016555	-0.6323	034566	0.0536	124444	-0.9233	134645	-0.0789
016565	-2.9317	034645	1.0856	124445	-0.8069	134646	0.3975
016655	-0.0103	034646	-0.8183	124446	-0.2238	144444	0.0418
016665	-0.8146	034666	1.9997	124465	0.8326	144446	-1.2806
016666	-0.6071	036666	-1.9807	124466	-0.8909	144646	-1.2338
024545	-0.3808	044646	-3.6831	124545	-1.0918		

Energy (Contract Nos. DE-FGO2-88ER40388 and DE-FG02-88ER40425). One of the authors (M.F.J.) wishes to thank Prof. Bruce French for his persistent encouragement and Prof. Haq Rizwan for providing the shell model computer code and his helpful instruction on how to use it.

APPENDIX: COMPLETE LIST OF *s-d* SHELL MATRIX ELEMENTS

In Tables VIII and IX we give a complete list of all 63 *s-d* shell matrix elements derived from the Bonn A and Bonn B potentials, respectively.

[1] R. Machleidt, Adv. Nucl. Phys. **19**, 189 (1989).
[2] R. Machleidt, K. Holinde, and C. Elster, Phys. Rep. **149**, 1 (1987).
[3] G. S. Chulick, C. Elster, R. Machleidt, A. Picklesimer, and R. M. Thaler, Phys. Rev. C **37**, 1549 (1988).
[4] R. V. Reid, Ann. Phys. (N.Y.) **50**, 411 (1968).
[5] M. Lacombe, B. Loiseau, J. M. Richard, R. Vinh Mau, J. Côté, P. Pires, and R. de Tourreil, Phys. Rev. C **21**, 861 (1980).
[6] R. B. Wiringa, R. A. Smith, and T. L. Ainsworth, Phys. Rev. C **29**, 1207 (1984).
[7] By definition, we call a potential "local" which, apart from the trivially nonlocal spin-orbit, $\mathbf{p}^2$, and/or quadratic spin-orbit operators, consists of local functions only.
[8] R. A. Brandenburg, G. S. Chulick, R. Machleidt, A. Picklesimer, and R. M. Thaler, Phys. Rev. C **37**, 1245 (1988).
[9] Kr. T. Kim, Y. E. Kim, D. J. Klepacki, R. A. Brandenburg, E. P. Harper, and R. Machleidt, Phys. Rev. C **38**, 2366 (1988).
[10] R. A. Brandenburg, G. S. Chulick, R. Machleidt, A. Picklesimer, and R. M. Thaler, Phys. Rev. C **37**, 781 (1988).
[11] B. D. Day, Comments Nucl. Part. Phys. **11**, 115 (1983).
[12] M. F. Jiang, R. Machleidt, and T. T. S. Kuo, Phys. Rev. C **41**, 2346 (1990).
[13] F. Coester, S. Cohen, B. D. Day, and C. M. Vincent, Phys. Rev. C **1**, 769 (1970).
[14] R. Brockmann and R. Machleidt, Phys. Lett. **149B**, 283 (1984); Phys. Rev. C **42**, 1965 (1990).
[15] T. T. S. Kuo and G. E. Brown, Nucl. Phys. **A85**, 40 (1966).
[16] J. Shurpin, T. T. S. Kuo, and D. Strottman, Nucl. Phys. **A408**, 310 (1983).
[17] B. H. Wildenthal, Prog. Part. Nucl. Phys. **11**, 5 (1984); B. A. Brown, W. A. Richter, R. E. Julies, and B. H. Wildenthal, Ann. Phys. (N.Y.) **182**, 191 (1988).
[18] W. W. Daehnick, Phys. Rep. **96**, 317 (1983).
[19] Some of our results have been published before in a Rapid Communication: M. F. Jiang, R. Machleidt, D. B. Stout, and T. T. S. Kuo, Phys. Rev. C **40**, R1857 (1989).
[20] A. Hosaka, K. I. Kubo, and H. Toki, Nucl. Phys. **A444**, 76 (1985).
[21] T. T. S. Kuo, S. Y. Lee, and K. F. Ratcliff, Nucl. Phys. **A176**, 65 (1971).
[22] T. T. S. Kuo, Annu. Rev. Nucl. Sci. **24**, 101 (1974).
[23] S. F. Tsai and T. T. S. Kuo, Phys. Lett. **39B**, 427 (1972).
[24] E. M. Krenciglowa, C. L. Kung, T. T. S. Kuo, and E. Osenes, Ann. Phys. (N.Y.) **101**, 154 (1976).
[25] J. B. French, E. C. Halbert, J. B. McGrory, and S. S. M. Wong, in *Advances in Nuclear Physics*, edited by M. Baranger and E. Vogt (Plenum, New York, 1969), Vol.3.
[26] H. M. Sommermann, H. Müther, K. C. Tam, T. T. S. Kuo, and A. Faessler, Phys. Rev. C **23**, 1765 (1981).
[27] J. P. Vary, P. V. Sauer, and C. W. Wong, Phys. Rev. C **4**, 81 (1971).
[28] We define $\chi^2 = \sum_{i=1}^{63}[M_{\rm Theo}(i) - M_{\rm Wild}(i)]^2$, where $M_{\rm Theo}(i)$ and $M_{\rm Wild}(i)$ denote the *s-d* shell matrix elements of the present theoretical calculations and of Wildenthal's empirical analysis [17], respectively.
[29] K. Holinde and R. Machleidt, Nucl. Phys. **A247**, 495 (1975).
[30] F. Ajzenberg-Selove, Nucl. Phys. **A475**, 1 (1987); P. M. Endt and C. Van der Leun, Nucl. Phys. **A310**, 1 (1978).
[31] T. Fortune *et al.*, J. Phys. G **11**, 1175 (1985).
[32] J. C. Sens *et al.*, Nucl. Phys. **A199**, 232 (1973); C. Rolfs *et al.*, *ibid.*, **A199**, 257 (1973).
[33] E. Maglione and L. Ferreira, Phys. Lett. B **262**, 179 (1991).